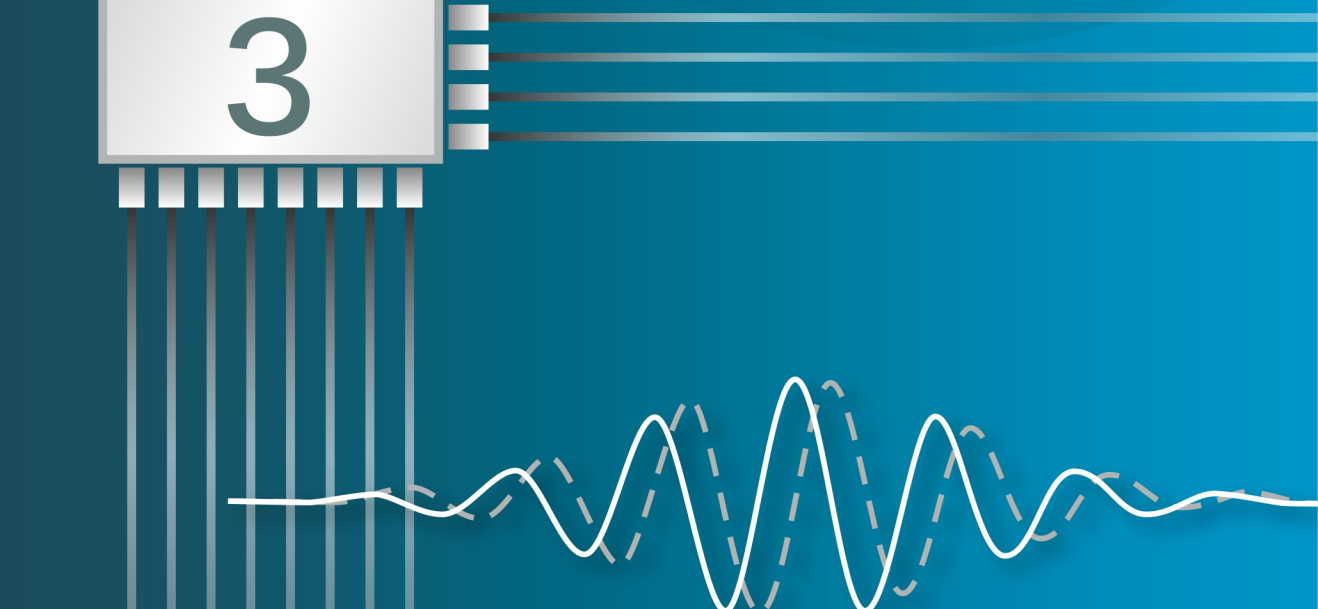


Sergey Y. Yurish Editor

Advances in Signal Processing



Advances in Signal Processing Book Series, Volume 3

Sergey Y. Yurish Editor

Advances in Signal Processing

Book Series, Volume 3



Sergey Y. Yurish *Editor*

Advances in Signal Processing: Reviews Book Series, Volume 3

Published by International Frequency Sensor Association (IFSA) Publishing, S. L., 2025 E-mail (for print book orders and customer service enquires): ifsa.books@sensorsportal.com

Visit our Home Page on http://www.sensorsportal.com

Advances in Signal Processing, Vol. 3 is an open access book which means that all content is freely available without charge to the user or his/her institution. Users are allowed to read, download, copy, distribute, print, search, or link to the full texts of the articles, or use them for any other lawful purpose, without asking prior permission from the publisher or the authors. This is in accordance with the BOAI definition of open access.

Neither the authors nor International Frequency Sensor Association Publishing accept any responsibility or liability for loss or damage occasioned to any person or property through using the material, instructions, methods or ideas contained herein, or acting or refraining from acting as a result of such use.

ISBN: 978-84-09-69173-9

BN-20250419-XX

BIC: UYS



Acknowledgments

As Editor I would like to express my undying gratitude to all authors, editorial staff, reviewers and others who actively participated in this book. We want also to express our gratitude to all their families, friends and colleagues for their help and understanding.

Chapter 1 Wearable PPG Sensors Applicable for Measurement in a Weak Magnetic Field Environment of an MRI Device

Jiří Přibil, Anna Přibilová and Ivan Frollo

1.1. Introduction

Magnetic resonance imaging (MRI) devices are widely used in modern clinical practice for non-invasive imaging of different parts of a human body. The MRI method can be useful also for creation of 3D human vocal tract models to examine dynamic changes in the shape of the vocal folds [1]. Next, the MRI tomography is suitable in the area of medical diagnostics – for classification and detection of Alzheimer's disease and other neurodegenerative disorders [2, 3]. The MRI tomographs are also often applied for monitoring of therapy progress after vocal fold cancer surgery, for evaluation of human knee cartilage [4], etc.

From the construction point of view, there exist two types of MRI scanners – the open-air ones used mainly for scanning of peripheral parts of the human body (arm, leg, knee, etc.) and the whole-body ones for widespread usage in MR imaging. MRI devices also differ in the working magnetic field used: open-air types usually work with a weak field (up to 0.2 T) [5], the whole-body types work with stronger basic magnetic fields (at present up to 11 T) [6]. Every MRI device consists of a gradient system to select x, y, and z slices of a tested object/subject situated inside the scanning area together with a radio frequency (RF) receiving/transmitting coil for generation of excitation pulses and catching an answer in the form of a free induction decay (FID) signal [7, 8]. In the open-air MRI system, planar gradient coils [9] are mostly used to minimize space requirements. The closed-bore (also called whole-body) MRI devices typically use cylindrical gradient coils distributed around the tube in which an examined person/object lies [10]. In both types of MRI equipment, rapid switching of large currents flowing through metal conductors of the gradient coils generates significant mechanical vibration and loud acoustic noises [8].

Jiří Přibil

Institute of Measurement Science, Slovak Academy of Sciences, Bratislava, Slovakia

Their intensity depends on the used type of a scan sequence and its parameters – sequence type, repetition time, echo time, slice orientation, etc. [7] as well as the volume inserted in the scanning area of the MRI device [11].

Due to electromagnetic compatibility and reduction of possible RF signal interference, the whole-body MRI scanning equipment is typically located inside a solid metal cage (often made from Cu plates). In the case of the open-air low field MRI device, this cage is made from a steel plate with thickness of about 2 mm with symmetrically placed small holes to eliminate electromagnetic field propagation to the surrounding space (a control room with an operator console, etc.) [9]. Therefore, using direct cable connection between sensors (measuring instruments) and evaluation/control unit (devices) located outside the shielding cage is practically very difficult to realize. On the other hand, the mentioned small holes in the steel plates practically enable wireless communication (via Wi-Fi or Bluetooth – BT) between the active scanning area and the control room with an operation console of the open-air MRI equipment. Investigations performed previously confirm the possibility of the data transfer through the closed door of the shielding metal cage [12], [13]. Therefore, the wireless communication based on BT connection is practically realizable and wearable sensors accessed by a bi-directional BT module are fully usable for this task. In addition, the performed analysis confirms that the BT communication inside the shielding cage does not interfere with the signals of RF coils and has no visible effect on the final quality of MR images [13]. On the other hand, the wearable sensors placed in the MRI scanner must not contain any metal part from ferromagnetic materials, to eliminate any interaction with a working magnetic field. It is important for preserving maximum quality of MR images without any artifacts. Due to strong RF disturbance, all parts of the sensor must be shielded by aluminium or brass boxes to prevent a damage of internal electronic circuits [13].

The general disadvantage of the MR scanning process consists in a fact that examined persons lying inside the running MRI scanner are exposed by noise and vibration causing them stress and other physiological or psychological negative effects. The level and impact on the scanned person depend on applied exposition time and intensity of vibration and acoustic noise. Negative impact to an examined person is manifested mainly by heart rate (HR) and arterial blood pressure (ABP) changes [14], which can be monitored during the MR scanning process. The HR values and their changes can be detected and evaluated from the signal sensed by an optical sensor working on a photoplethysmography (PPG) principle, while the systolic or diastolic blood pressure values are usually measured by a blood pressure monitor device (BPM) [15]. The PPG measurement uses an optical sensor for non-invasive pickup of vital functions of the vascular system from the skin [16] by detecting blood volume changes inside the tissue. Obtained PPG signals can be next used to determine other specific parameters applicable in systems for medical assessment [17], and/or utilized for biometric authentication [18]. At present, several cuffless techniques based on estimation of ABP values directly from one or more-channel PPG waves sensed simultaneously [19] are often applied. These methods use several time domain parameters, energetic, and spectral features determined from the recorded PPG waveform(s). The ABP values may be assessed with higher precision when are used – typical representatives of these parameters are the pulse transmission time (PTT) and the pulse wave velocity

(PWV) [20]. If PTT is used in addition to PPG, the estimated BP values are more accurate [21, 22] because of linear relation between the PTT and ABP values [23, 24].

This chapter describes realization, testing and practical experiments with developed special prototypes of wearable PPG sensors applicable for real-time sensing of one, two, and/or thee-channel PPG waves with wireless data transfer to a control device – all in the environment of the open-air low field MRI tomograph. Basic working principles and realizations of the optical part of the PPG sensor are also discussed here. The chapter continues with description of structures and basic functional parts of the developed wearable sensors. Next, the communication and control strategy used for real-time data transfer and PPG samples storage in a control device is discussed. Then the chapter follows a detailed description of created control application for Windows platform – all operating elements on the control panel are explained here. Description of the method used for determination of different parameters from the sensed PPG wave(s) with respect to unipolar representation of the PPG signal(s) is presented next. Last but not least, the comparative measurements performed with the certified commercial pulse oximeter (OXI) device and the clinical BPM device for evaluation of stability and precision of the determined HR values was mentioned in this study.

1.2. A PPG Sensor: Principle, Structure, and Function

1.2.1. Basic Description of Wearable PPG Sensors

In general, an optical sensor working on a photoplethysmography principle can operate in a transmittance or a reflectance mode [25]. The transmittance type of a sensor probe has usually a form of a finger ring or an ear clip with a light source (one or more LED elements) and a photo detector (PD) placed on opposite sides of the sensed human tissue – see a principal example in Fig. 1.1a). For the reflectance sensor type holds that the PD element measures the intensity of the light reflected from the skin and it is placed on the same side of the skin surface as the light source transmitter – see principal examples in Fig. 1.1b). This type an optical sensor is placed mainly on fingers or a wrist, typically fixed by an elastic/textile ribbon or it is integrated as a part of different wearable devices – fitness bracelets, smart watches, etc. In both cases, the signal from PD that is next amplified and filtered represents a dynamic component – DC part of the photoplethysmography signal [26]. The PPG signal consists of typical systolic and diastolic peaks (an example in Fig. 1.1c). The systolic peak on the PPG wave directly corresponds with a heart activity – it is derived from the *R* peak of the electrocardiogram (ECG).

The wearable PPG sensor enabling the real-time, continual PPG signal measurement consists principally of four basic functional parts:

- a microcontroller or DSP processor board with integrated A/D convertors, including also a hardware SPI/I2C port, and an UART to USB interface;
- a BT receiver/transmitter for serial bi-directional communication with control device(s);

- one or more optical pulse PPG sensors working in a reflectance or transmittance mode with fully integrated analogue interfaces;
- a power supply part as shown in a principal diagram of a three-channel PPG sensor structure presented in Fig. 1.2.

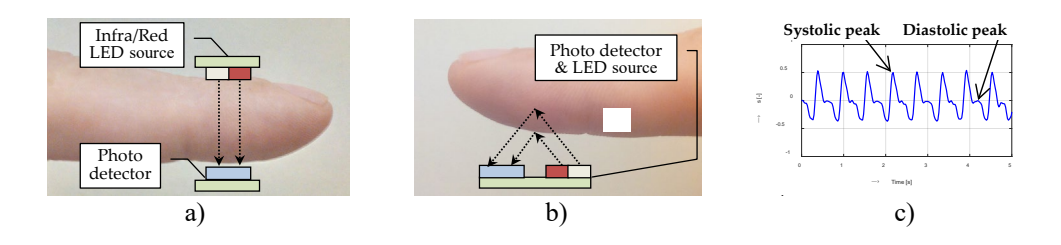


Fig. 1.1. Basic principle of PPG sensors working in: a) Transmittance; b) Reflectance modes; c) Example of sensed PPG wave.

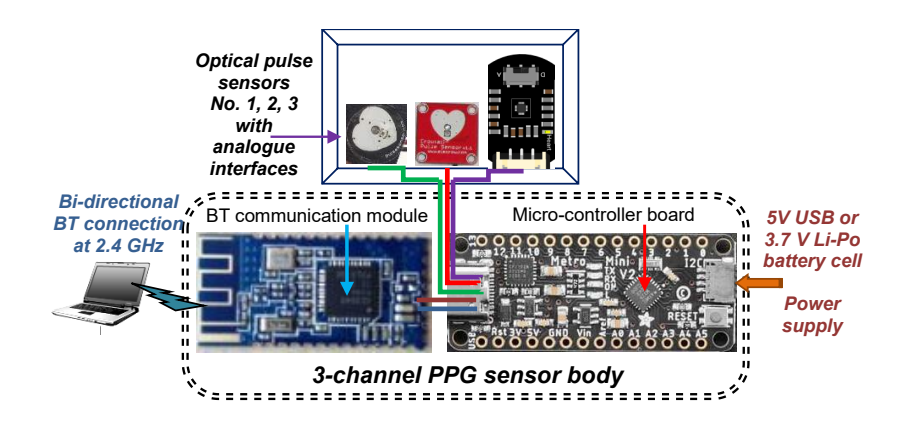


Fig. 1.2. Principal structure diagram of a wearable three-channel PPG sensor.

The power supplying the whole sensor can be realized using the rechargeable polymer-lithium-ion (Li-Po) cells with output voltage of 3.7 V, or by 5 V external power banks via the USB port independence of used micro-controller board (using 3.3 V or 5 V logic levels). The BT modules as well as the optical pulse sensors usually can work with both voltage levels without any additional signal conversion requirements. The capacity of the power supply device used finally depends first of all on the resulting DC current of the whole sensor, the required time duration for continual measurement, the maximum sampling frequency f_S for sensing of PPG signal(s), and the maximum serial communication rate for real-time data transfer to the control device. Processors working at the voltage level of 3.3 V have typically the clock frequency of 8 MHz, so the maximum $f_S = 500$ Hz and communication at the baud rate of 57600 bps could be achieved. In this case, using of Li-Po batteries with capacity from 125 to 750 mAh is proper for normal

experimental purpose. Microcontrollers and processors operating at the 5 V voltage level work usually with $f_{\rm CLK} = 16$ MHz, so higher sampling frequency up to 1 kHz and higher serial communication rate of 115200 bps could be reached. On the other hand, this type of PPG sensor has also higher requirements on the capacity of the powering part. For long-time experiments the power banks with capacity from 2000 to 5000 mAh are suitable to guarantee safety and stable supplying for the whole-time duration of the measurement.

A relatively high sampling frequency of at least 500 Hz is necessary to perform the analysis of morphological features of the individual PPG pulse waves [27] as well as to determine PTT and PWV parameters with high precision. On the other hand, commercially available PPG devices typically sample the PPG signal at low frequencies (from 50 to 100 Hz) [25]. Lower sampling frequencies are also suitable for continual long-term acquisition of the PPG signal, e.g., sampling at 128 Hz was used by [17] for atrial fibrillation monitoring with the PPG sensor on a wrist.

The whole sensor can work in "Slave" or "Master" mode depending on the sensing and data transmission strategy used. We are oriented to the control strategy when the PPG sensor works as a "slave", i.e. after initialization it waits for commands from the master external device (notebook, desktop PC, etc.) via the BT communication. The service program on a microcontroller board enables adjustment of the time delay $T_{\rm INT}$ (internal interrupt clock) to read the analog signal and make A/D conversion. It means analogue signals from the optical PPG parts are sensed at the sampling frequency f_S corresponding to the chosen T_{INT} value. Next, the data block size N_{MEAS} of 16-bit PPG signal samples are set for transmission to the control device. Finally, the number of used channels – number of optical pulse sensors to be read – must be adjusted and size of head communication data buffers must be set. On the side of a control device, the application must control acquisition of one or more-channel PPG signals, their processing, and data storage. This application was mostly created for Windows platform working on standard PC desktop or portable laptop devices. It is also possible to create an application under Android platform for implementation on mobile devices (tablets and/or smartphones). Practically, the control application performs two basic tasks:

- 1. real-time monitoring and displaying of PPG signals picked up currently from one or more optical PPG sensors;
- 2. continuous PPG signal measurement with the selected sampling frequency f_S in data blocks of N_{MEAS} samples.

Within the real-time PPG signal(s) measurement following operations can be also performed:

- direct storing the received samples of the PPG signal to a file on the disk of the master device without any next processing using the commands "Start" and "Stop" sent manually by the user;
- storing the PPG signal samples to an internal memory buffer enabling to perform post-processing operations as filtering and HR determination; in this way the modified data can be stored off-line to the file(s) by the application user.

Operating in the measurement mode denotes that the data block with chosen dimension and structure of PPG signal samples from one or more optical pulse sensor(s) are automatically transmitted to a control device in the frame of real-time operation. The sensed PPG signal(s) are subsequently stored in a Wave format (with 16-bit quantization, mono, PCM coding). These PPG wave records can be further processed and analyzed off-line, for example in the Matlab program environment.

1.2.1. Description of Realized Wearable PPG Sensors

In the frame of our long-term research aim to apply PPG sensors in the measurement inside the scanning low-field MRI tomograph, several special prototypes were developed. The main motivation was to realize wearable PPG sensors representing a low-cost solution, but fully operational for our experimental purpose. Five prototypes of PPG sensors were subsequently realized within last five years – three one-channel prototypes, one consisting of three optical pulse sensor parts, and one prototype enabling sensing of a two-channel PPG signal in parallel (further called as "PPG-EP", "PPG-PS1", "PPG-BLE", "PPG-2Tp", and "PPG-3p" – see details in Table 1). They next differ in the type of optical parts (of the reflectance/transmittance design), type of BT communication module, and used voltage level for power supply.

To eliminate the mentioned interaction with the magnetic field and prevent possible disturbance in electromagnetic compatibility inside the running MRI equipment, the processor board with the BT module as well as the optical sensor are covered in two separate aluminium shielding boxes as documented by the photos in Fig. 1.3.

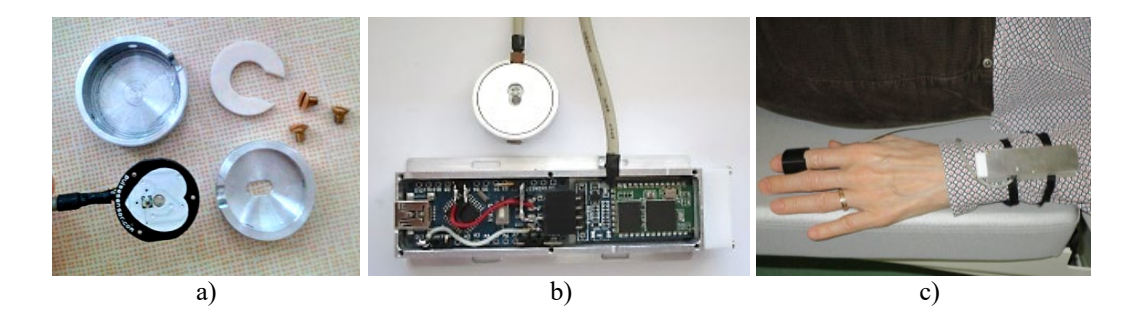


Fig. 1.3. Example of assembling and covering of: a) Optical Pulse sensor; b) Micro-controller board with BT communication module (sensor's body) with closed optical sensor part; c) Closed body and optical part of the PPG sensor worn on a left hand without power supplying [13].

On the side of the micro-controller part, all sensors have been realized with the help of the open-source development platform Arduino boards [28]) based on the 8-bit processor ATmega328 by Atmel company with integrated eight 10-bit A/D converters. It means that the sensed PPG signal has the theoretical maximum value given by the number of bits of the A/D convertor and practically denoted by the used voltage level (5/3.3 V) of the power supply. Following types of Arduino compatible boards were stepwise used:

- 1. Arduino Uno ver. 3.0 board [29] or Nano ver. 3.0 board [30] based on the Atmel processor ATmega328P with $f_{\rm CLK}=16$ MHz (operating at 5 V level) with an integrated USB interface for serial programming and testing;
- 2. Arduino Pro Mini v. 2.0 board [31] also with the processor ATmega328 but without the USB interface and running at $f_{CLK} = 8$ MHz and operating at 3.3 V level;
- 3. Adafruit Metro Mini 328 board (Arduino compatible) based on the processor ATmega328P, including also hardware SPI and I2C ports, and an UART to USB interface [32].

For wireless communication between the control device and the PPG sensor, two types of BT modules working at 2.4 GHz were used:

- BT communication module HC-06 (Waveshare 4328 [33]) fully compatible with the Arduino platform, working in BT 2.0 standard with the maximum baud rate of 115200 bps;
- BT module MLT-BT05 by Techonics, Ltd. [34], working in BT4.1 BLE (low energy) standard, supporting also the serial baud rate up to 115200 bps.

The PPG also sensors differ in the used optical pulse sensor parts. Following three types of optical sensors with fully integrated analogue interfaces were applied in the developed PPG sensors:

- the Pulse Sensor Amped (Adafruit 1093) by Adafruit Industries [35];
- the Crowtail-Pulse Sensor (ER-CT010712P) by Elecrow Company [36];
- the Gravity Heart Rate Sensor (SEN0203) by Zhiwei Robotics Corp. [37].

Due to a reflectance principle, the sensor's photo detector and light source elements are placed on the same side of the skin surface on fingers or a wrist fixed by an elastic/textile ribbon. Next, two types of sensors working on the transmittance principle were applied in the PPG sensor prototypes:

- the Easy Pulse sensor v 1.1 analogue module (ER-CDE10301E) by Embedded Lab, with the optical sensor HRM-2511E by Kyoto Electronic Company [38],
- the Easy Pulse Mikro a micro Bus compatible pulse sensor (designed by Embedded Lab) including the PPG optical pulse sensor ER-CDE17527M by Kyoto Electronic Company [39].

While the reflectance sensors have fully integrated analogue interface on the main board together with LED source and photo detector elements (see photos of Adafruit 1093, ER-CT010712P, and SEN0203 sensors in Fig. 1.4a-c), the transmittance types have an analogue interface located on a separate board and an optical part practically realized in the form of a rubber finger ring – see an example of HW realization in Fig. 1.4d-e.

With respect to expected long-term measurement experiments or for using multi-channel PPG sensor realizations, the whole sensor was powered via the USB port by the 5 V power bank THAZER (with 2200 mAh capacity), or by RealPower PB-4000 (4000 mAh). For short-time experiments using 3.3 V level devices, the 3.7 V textile battery (rechargeable Li-Po cell) with capacity of 125 mAh (for one-channel sensors) or with the capacity of 750 mAh (in the case of two-channels sensor) were applied, as documented by photos in Fig. 1.5. Differences in the architecture, the basic components used, the electrical and mechanical parameters of all developed PPG sensor prototypes are shown in Table 1.1.

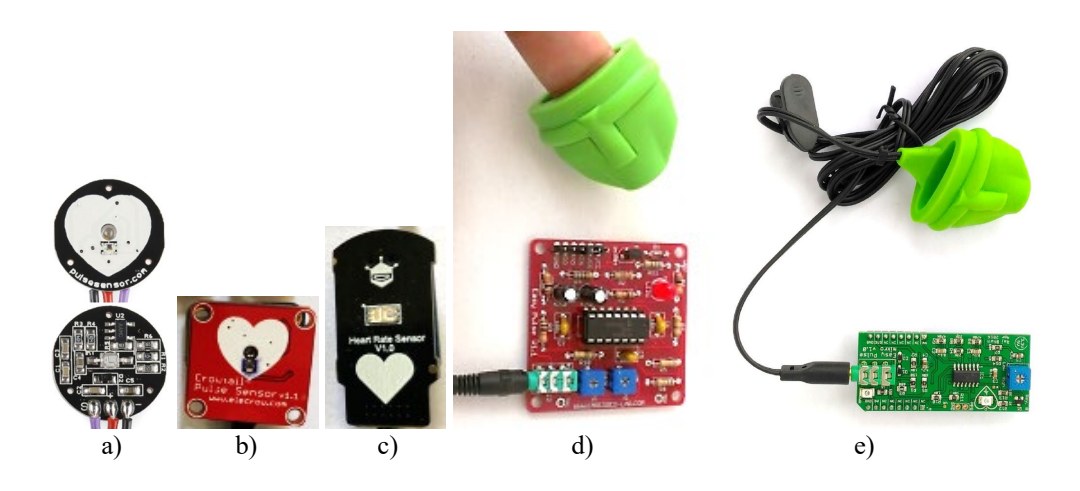


Fig. 1.4. Example of HW realization of commercial heart pulse sensors: a) Front and back side of the Pulse Sensor Amped [35]; b) Front side of Crowtail-Pulse Sensor [36]; c) Front side of the Gravity Heart Rate Sensor [37]; d) Easy Pulse sensor v 1.1 analogue module [38]; e) Analogue board Easy Pulse Mikro connected with the ER-CDE17527M optical sensor [39].

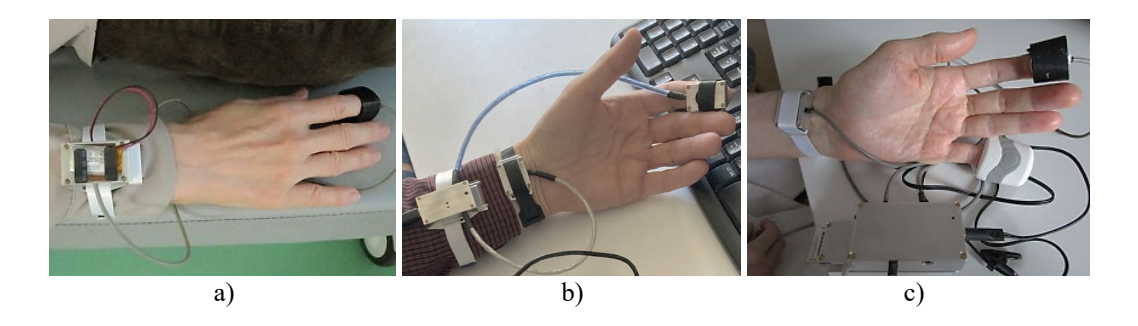


Fig. 1.5. Example of realization, wearing and powering of developed PPG sensors: a) One-channel protype with mounted a 3.7 V Li-Po battery cell; b) Two-channel protype using two reflectance optical sensors; c) Three-channel protype consisting of one transmittance and two reflectance optical sensors; both multi-channels realizations are supplied by a 5 V power bank [13].

Table 1.1. Differences in architecture, basic components, mechanical and electrical parameters, for all five developed PPG sensor prototypes.

| Params. | Prototype name | | | | | | |
|-------------------------------|----------------|---------------|--------------------|---------------------------|--|--|--|
| | PPG-EP | PPG-PS1 | PPG-BLE | PPG-2Tp | PPG-3p | | |
| No of channels | 1 | 1 | 1 | 2 | 3 | | |
| Optical sensor(s) | HRM-2511E | Adafruit 1093 | Adafruit 1093 | ER-CT010712P + SEN0203 | 2x Adafruit 1093 + ER- CDE17527M | | |
| Working mode | Trans. | Reflect. | Reflect. | 2x reflect. | 2x reflect. + 1x trans. | | |
| Arduino board | Uno v.3.0 | Nano v.3.0 | Pro Mini v. 2.0 | Metro Mini 328 | Nano v.3.3 | | |
| BT module | HC-06 | HC-06 | MLT-BT05 | MLT-BT05 | HC-06 | | |
| Voltage level | 5 V | 5 V | 3.3 V | 3.3/5 V | 5 V | | |
| Mean DC current | 60 | 26 | 14 | 20/31 | 38 | | |
| Procs. f_{CLK} | 16 MHz | 16 MHz | 8 MHz | 8/16 MHz | 16 MHz | | |
| Body dimensions (L×W×H) | 105×70×80 mm | 80×20×10 mm | 40×25×15 mm | 46×25×12 mm | 80×33×30 mm | | |
| Body weight | 445 g | 55 g | 40 g ¹⁾ | 45 g ¹⁾ | 180 g ²⁾ | | |

¹⁾ without mounted a Li-Po battery cell

3.2.2. Description of the Control Application Based on Windows Platform

Originally, each of the PPG sensors developed sequentially had an own Windows application for a control device. At present, one universal application called *PPGsensUniv.exe* was built. It enables control of one, two, or three-channel PPG signal acquisition, post-processing operation and PPG records storage for all of five realized PPG sensor prototypes, and communication with different types of PPG sensors in three functional modes:

- 1. <u>Off-line</u>, i.e., without any BT communication only stored PPG waves can be shown, analyzed, and processed;
- 2. <u>Automatic</u>, i.e., with automatic connection to a pre-defined type of a PPG sensor (by initial setting of program parameters stored in *.INI files for each of sensor types) real-time PPG signal monitoring and/or continual measurement in data blocks (including subsequent storing of received data to an external file);
- 3. <u>Manual</u>, beginning with the application start without BT connection, proceeding with a manually established connection to a chosen type of a PPG sensor and communication parameters (serial channel type, baud rate, BT 2.0/BT 4.1 BLE protocol, etc.) working in a similar way as in the automatic mode.

Within the manual function it is also possible to manually disconnect the currently chosen PPG sensors and/or create a connection with another PPG sensor using different

²⁾ together with the analogue board EasyPulse Mikro

parameters. Due to the real-time requirement, only the following settings are possible: $T_{\text{INT}} = \{10, 8, 5, 4, 2, \text{ and } 1 \text{ ms}\}$ representing the sampling frequencies $f_{\text{S}} = \{100, 125, 250, 500, \text{ and } 1000 \text{ Hz}\}$ in the data blocks of $N_{\text{MEAS}} = \{1\text{k}, 4\text{k}, 16\text{k}, 32\text{k}, \text{ and } 64\text{k}\}$ of 16-bit samples after A/D conversion.

An example of a screen copy of the main control window of the application *PPGsensUniv* (version 1.03, actually connected with the three-channel PPG sensor PPG-3p) is shown in Fig. 1.6. The main window can be divided into seven areas "A"-"G" in correspondence with different control functions and operations:

- 1. Area "A" place for displaying the sensed PPG signals together with their selected signal thresholds for systolic peak detection and HR determination operations (see a green dashed line); the threshold can be set automatically or manually by a slider tool located on the right of the graphics area. Next, we can see the displayed sequence of HR values determined per a heart pulse period from the selected PPG channel (drawn at bottom, by a green solid line). This display area is also used as a graphical output for function during the monitoring operation. In this case, the HR sequence is shown after stopping this process (from the last 1k-sample data block).
- 2. Area "B" field of PPG channel parameters enabling: inversion operation (buttons \underline{Inv}), signal amplification (buttons \underline{G}), and absolute offset shift (buttons \underline{O}) for each of the channels separately.
- 3. Area "C" upper part consisting of switches to select the active PPG channel for HR determination and panel with the mean HR value for the whole PPG record; lower part with switches for PPG signal filtering and automatic threshold calibration.
- 4. Area "D" set of buttons for managing and manual controls of graphical output (zoom in/out, redraw, clear and initialize the drawing area).
- 5. Area "E" part for saving of the currently selected PPG signal(s) to an output file (in binary or ASCII format) or loading a previously stored file with PPG signals. In the right part, there are also placed panels with information about parameters of the currently sensed or loaded PPG signals: number of channels, length of data in samples, used sampling frequency.
- 6. Area "F" the main part for managing and control of PPG signal monitoring, real-time receiving of PPG signal samples to an internal memory, or direct storing to an output file. Next, this area consists of buttons for starting/finishing ($\underline{Monit/End}$) the monitoring operation and one button (\underline{Read}) for manual start of the automatic PPG signal pickup. There are also info panels about the chosen number of samples to be sensed (N_{MEAS}), the time interrupt T_{INT} in ms to take a PPG signal sample(s) together with automatically adjusting of f_{S} in Hz), and the pre-calculated time duration value in seconds for the actual sensing operation.
- 7. Area "G" the system setting and info part showing current status of connection with a chosen type of PPG sensor (name of sensor, associated serial communication channel and data transfer rate), pop-up selector for choice of PPG sensor, button for calling of a dialog window to set other system parameters, and finally the exit button for closing

the whole application (after closing all BT connections and open graphical/dialog windows).

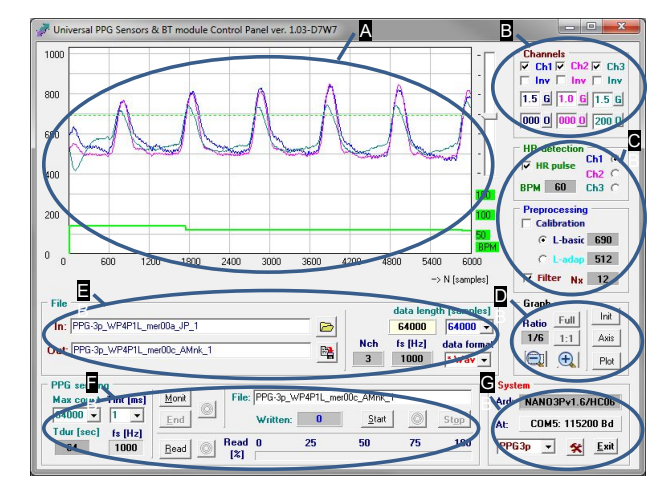


Fig. 1.6. Screen copy of the control application *PPGsensUniv* – actually selected function with a three-channel sensor *PPG-3p*.

The activated parameter setting window with shown listing during establishing of the BT connection with the PPG sensor working at the standard 4.1 BLE – transmitted and received AT commands for MLT-BT05 module can be seen in Fig. 1.7a. A simple communication during connection creation using the BT 2.0 standard for HC-06 BT module is shown in Fig. 1.7b. This window of communication parameters also enables setting of an actual serial channel (associated with a paired BT device), a current serial rate in bauds, a time duration for waiting response from the slave device, and the data format for commands and data transfer (text in ASCII or binary in 16-bit words). For the correct functionality with a chosen number of a serial channel, the BT pairing process must be performed first in the Windows control panel setting (outside of this application) – see an example in Fig. 1.8.

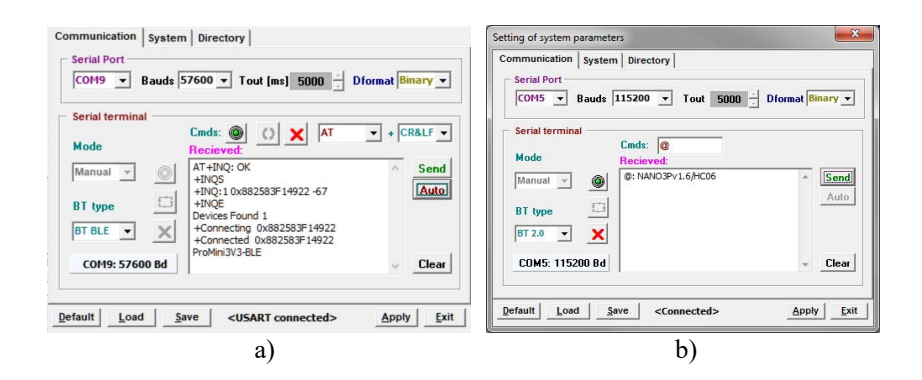


Fig. 1.7. Screen copy of the dialog window for setting of system parameters currently displaying a section of BT connection and communication for: a) module MLT-BT05 with BT 4.1 BLE protocol [13], b) module HC06 running at BT2.0 standard.

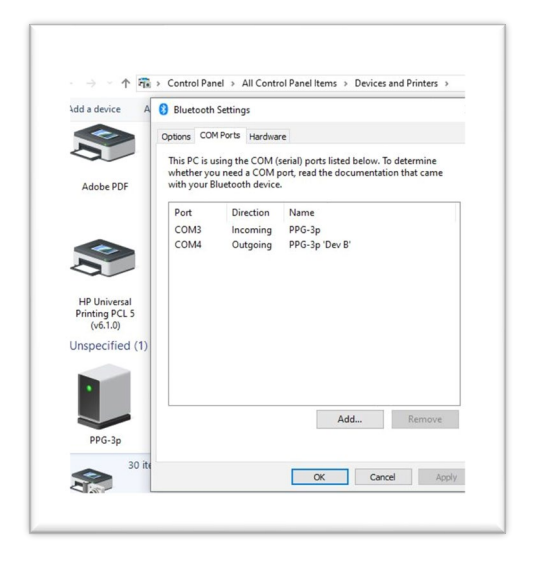


Fig. 1.8. Example of control panel in Windows 10 OS – the PPG3p sensor is associated with the system serial channel COM4.

1.3. PPG Signal Properties, Processing, and Analysis

1.3.1. Basic Description of PPG Signal Properties and Processing

From the physical principle follows that a great part of the PPG signal is composed of a direct current (DC) component corresponding to the whole blood volume of an examined tissue. The superimposed alternating current (AC) component follows the beating of the heart, so it carries also vital information including the heart rate. Its magnitude is much smaller (typically about 2-3 % of the DC component), as can be seen in a principal diagram in Fig. 1.9a.

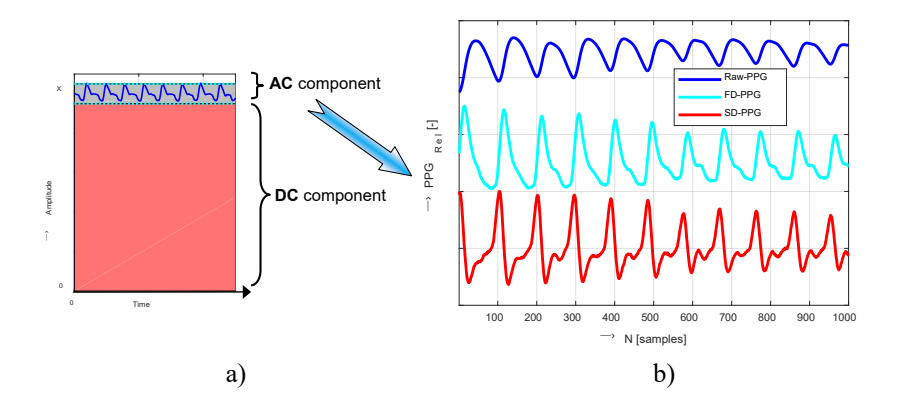


Fig. 1.9. Principal structure of a PPG signal: a) Superposition of AC and DC components, b) 1k-sample example of PPG wave in three basic forms (raw PPG, FD-PPG, and SD-PPG).

A crucial step in the PPG pulse wave analysis is calculation of signal derivatives that may be used for determination of pulse wave features. The original pulse wave – (raw PPG), its first derivative (FD-PPG) – called also as velocity photoplethysmogram, and its second derivative (SD-PPG) – known as acceleration photoplethysmogram, are practically taken, processed, and analyzed [26]. The mentioned systolic and diastolic peaks are present in each cycle of the PPG wave (see the demonstration example of sensed PPG wave in Fig. 1.1c). They must be detected and localized for the purpose of further analysis. While the raw PPG signal is not suitable for local maxima determination, the FD-PPG and particularly the SD-PPG waves are more informative due to more pronounced local extrema as shows an example in Fig. 1.9b.

Generally, the picked-up PPG signal has an amplitude modulation with a partially linear trend (LT), it usually contains a superimposed noise component, and sometimes it is partially disturbed or degraded. Therefore, the sensed PPG signal must be pre-processed prior to further practical use. In the frame of the de-trending operation, the LT is calculated (usually by the mean square method) and applied within the LT removal procedure. Then, the PPG signal must be smoothed to eliminate local artifacts caused by signal noise or disturbance. In a lot of cases it seems to be sufficient to apply a moving average (MA) filter with the window length $w_{\rm MA} = 2Nx+1$. In this way we can obtain a clean PPG waveform describing actual condition of the cardiovascular system of a tested person. Three groups of PPG wave parameters are typically determined within the PPG signal analysis:

- 1. Temporal and energetic parameters: amplitude, signal range, and signal modulation;
- 2. Heart rate values and their statistical properties (variance, etc.);
- 3. Heart pulse transmission parameters pulse transmission time (PTT) and pulse wave velocity (PWV).

1.3.2. Determination of PPG Wave Parameters

Most used algorithms work with a PPG wave in a relative bipolar presentation, such that the PPG signal lies in the range of ± 1 . As all the developed prototypes of PPG sensors produce absolute signals in the range of ± 1 024, different approaches must be used or adopted in this situation. Because the analogue interface of optical sensors performs de-trending of the PPG signal during its cascade processing, this task cannot be solved in this case. Smoothing of sensed PPG signals is carried out by the MA filter with the N_x parameter chosen in dependence on the currently used sampling frequency. This operation is applied only once when the whole data block is transferred to the memory of the main control application. It means practically, that the PPG signal(s) continually displayed within the monitoring mode is not any filtered.

Analysis of the PPG signal pre-processed in this way starts with localization of systolic peaks P_{SYS} and heart pulse periods (T_{HP}). Our proposed method works in four steps:

- 1. Setting of the PPG signal threshold L_{THRESH} ;
- 2. Binary clipping of the input pulse wave;

- 3. Localization of the systolic peaks P_{SYS} ;
- 4. Determination of the heart pulse periods $T_{\rm HP}$.

The level threshold can be set either manually individually for each of the processed PPG signals or adaptively – typically at one-third from the systolic pulse peak. During processing of the PPG signal with the length of P samples, the clipping operation produces a sequence $c_{PPG}(i)$ of values 1/0 corresponding to the input signal samples above/below the adjusted threshold level L_{THRESH} as

$$c_{PPG}(i) = \begin{cases} 1 & y(i) \ge L_{TRESH} \\ 0 & y(i) < L_{TRESH} \end{cases}, 1 \le i \le P$$

$$(1.1)$$

The position of each of the systolic peaks $P_{\rm SYS}$ is basically determined as the middle of every T_1 interval. To localize $P_{\rm SYS}$ with higher accuracy it is necessary to pick up PPG signals with higher sampling frequency $f_{\rm S}$. Therefore, the systolic peak position is finally set as the local maximum found in the T_1 interval – see an example in Fig. 1.10. The heart pulse periods $T_{\rm HP}$ are determined from this clipped sequence as the length of two adjacent continual parts of ones (with T_1 samples) and zeros (T_0 samples), i.e. $T_{\rm HP} = T_1 + T_0$.

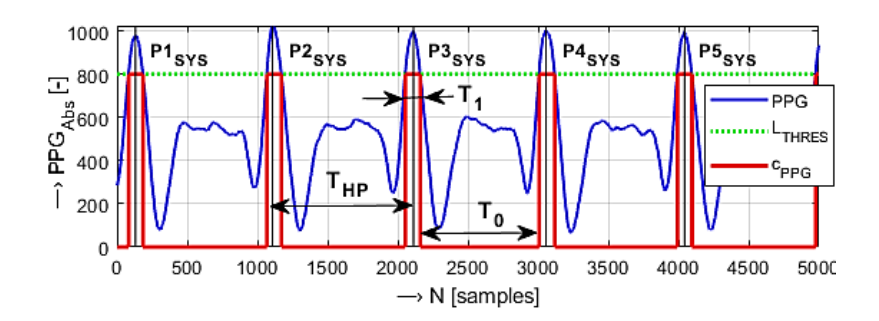


Fig. 1.10. An example of 5k-sample part of one-channel PPG signal together with: clipping sequence c_{PPG} , signed heart pulse period T_{HP} , and lengths of T_1 , T_0 for the systolic pulse P3_{SYS}; $L_{\text{THRES}} = 800$.

Obtained systolic peak positions and lengths of heart pulse periods are subsequently used for determination of other PPG wave features. To obtain temporal and energetic parameters, the following operations and calculations are performed:

1. Finding of maximum and minimum levels of localized systolic peaks (Lsp_{MAX} and Lsp_{MIN}) together with the whole signal offset level (L_{OFS}). These levels are needed for calculation of the mean absolute systolic peak amplitude (SP_{AMPL}), using the mean signal offset value μL_{OFS} as

$$SP_{AMPL} = (Lsp_{MAX} + Lsp_{MIN})/2 - \mu L_{OFS};$$
 (1.2)

2. Then, the relative systolic peak ripple SP_{RIPP} in percentage of a PPG wave (see demonstration example in Fig. 1.11) is calculated using the following formula

$$SP_{RIPP} = (Lsp_{MAX} - Lsp_{MIN})/Lsp_{MAX} \times 100;$$
 (1.3)

3. Finally, the relative signal range (PPG_{RANGE}) in percentage can be determined from the absolute systolic peak amplitude SP_{AMPL} as

$$PPG_{RANGE} = SP_{AMPL} / AD_{NRES} \times 100,$$
 (1.4)

where the AD_{NRES} represents the numerical resolution of the currently used A/D converter. In our case, for all analyzed PPG signals the AD_{NRES} value was equal to 1024, since 10-bit A/Ds were used for digitalization of the analogue signal from the optical sensor (2¹⁰ = 1024).

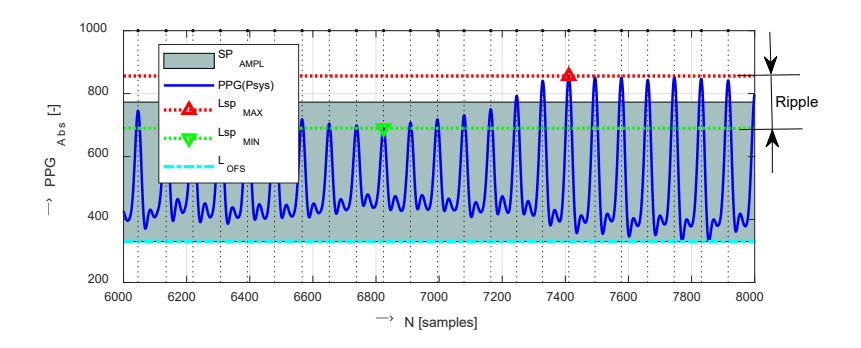


Fig. 1.11. An example of 2-k sample part of a PPG signal with localized systolic peaks P_{SYS} and their mean amplitude SP_{AMPL} , determined $L_{\text{SP}_{\text{MAX}}}$, $L_{\text{SP}_{\text{MIN}}}$, and L_{OFS} levels used for ripple calculation.

Using the sampling frequency f_S in Hz and the heart pulse period T_{HP} in samples, the heart rate HR in min⁻¹ can be easily calculated as

$$HR = 60 \times f_S / T_{HP} \tag{1.5}$$

The heart pulse transmission parameters are determined from two PPG waves (PPG_A, PPG_B) sensed in parallel. It is important to localize precisely the systolic peak positions P_{SYS} in both PPG signals and to measure correctly differences between P_{SYS} in samples ($\Delta P_{SYSa,b}$) – see a demonstration example for a two channel PPG signal in Fig. 1.12.

For the applied sampling frequency f_S expressed in Hz, the pulse transit time parameter (PTT in ms) is calculated as

$$PTT = \Delta P_{SYS} / f_{S} \tag{1.6}$$

When we know the distance between locations of the optical PPG sensors (Dx in m) and the pulse transit time parameter (PTT in s), then the pulse wave velocity parameter (PWV in m/s) [20] is calculated as follows

$$PWV = Dx/PTT (1.7)$$

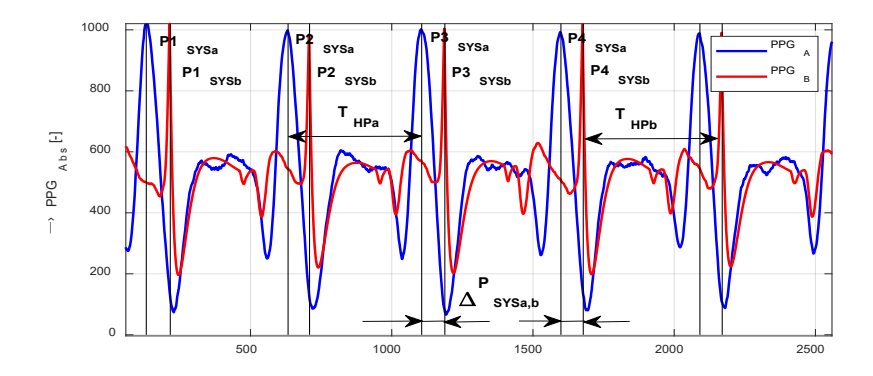


Fig. 1.12. An example of 2.5k-sample parts of two PPG waves sensed in parallel (PPG_A and PPG_B) with denoted heart pulse periods $T_{\text{HPa,b}}$ and determined time differences between systolic pulses $\Delta P_{\text{SYSa.b}}$.

The final accuracy of the determined PWV values depends partially also on the absolute error of practical measurement of the distances Dx. The fist optical sensor is usually mounted on a wrist, and the second one on finger(s), so the Dx distance can be easily measured along the horizontal line as follows from the arrangement photo in Fig. 1.13. More sophisticated method measures the Dx as a length of the path between the wrist and the fingers along the blood arteries. This methodology follows from the fact that the blood really flows in this way in a measured hand. The main disadvantage of this measurement approach is its great individual-dependence. In addition, the distance Dx could be finally measured with lower accuracy – practically comparable with the first easy way and will not bring better results.

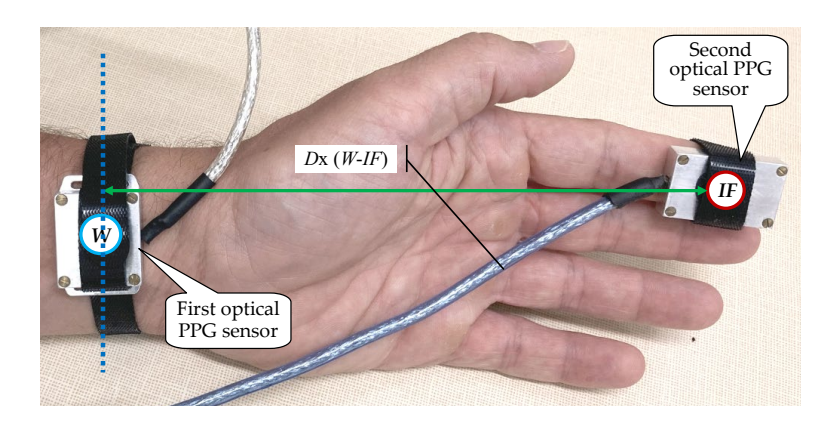


Fig. 1.13. An example of arrangement for two-channel PPG signal acquisition by optical sensors located on a wrist (*W*) and an index finger (*IF*) at a distance *Dx* measured along the horizontal line.

The obtained PPG wave parameters are then statistically processed to get one final representative value for direct numerical comparison. The histograms are useful to map

and describe distribution of their values. When the probability distribution of the analyzed parameter has non-Gaussian character, then using the mean or median values does not provide a correct final result. In this case it is better to determine the value h_{MAX} corresponding to the maximum occurrence o_{MAX} [%] in the histogram, however, o_{MAX} must be significant – in praxis is usually sufficient to use $o_{\text{MAX}} \ge 20$ %. Otherwise, higher differences between h_{MAX} and mean values are present (as shown by histograms in Fig. 1.14), and better precision is practically achieved by calculation using the median method.

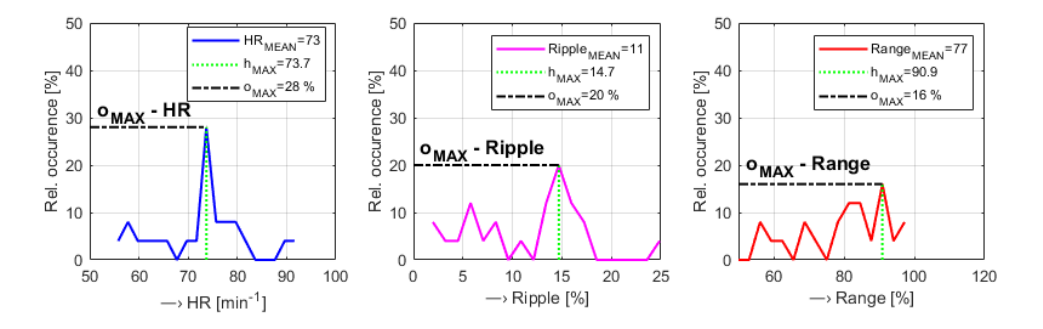


Fig. 1.14. Histograms demonstrating differences between calculated mean and h_{MAX} values in dependence on maximum occurrence o_{MAX} for: HR, systolic peak ripple, and relative signal range parameters (from left to right).

1.4. Evaluation of Precision of Realized PPG Sensors

To evaluate the precision and stability of HR values determined from sensed PPG signals (HR_{PPG}) , two types of comparative measurements of HR values (HR_{CMP}) were performed:

- comparative measurement of HR values determined from PPG signals sensed by three one-channel PPG sensors together with parallel measurement by a certified OXI device;
- 2. comparison of the accuracy and stability of HR values determined from PPG signals sensed by all five developed wearable PPG sensors the HR values were measured in parallel by a commercial BPM device used also in medical practice.

When the comparative HR measurement by a BPM device is applied, the $HR_{\rm CMP}$ parameter represents one value $HR_{\rm BPM}$ obtained for the whole measuring interval with duration $T_{\rm DUR}$. In the case of using an oximeter which produces continual values of HR during the whole measurement, the $HR_{\rm OXI}$ is defined as the mean value. To enumerate the overall estimation accuracy, the percentage relative differential parameter $HR_{\rm DIFF}$ – relative to the mean value of $HR_{\rm PPG}$ sequence ($\mu HR_{\rm PPG}$) – can be calculated as

$$HR_{\text{DIFF}} = (HR_{\text{CMP}} - HR_{\text{PPG}}) / \mu HR_{\text{PPG}} \times 100$$
 (1.8)

The obtained accuracy is compared with other related works using the mean absolute error (MAE) parameter calculated as a mean of a simple absolute difference $\Delta HR_{\rm OXI,BPM} = HR_{\rm CMP} - HR_{\rm PPG}$ in min⁻¹. For mapping of correlations between the measured $HR_{\rm CMP}$ and the determined $HR_{\rm PPG}$ values, the scatter plots can be used. For this purpose, the Pearson correlation coefficient R is calculated as

$$R(X,Y) = \frac{1}{N-1} \sum_{n=1}^{N} \left(\left(X_{n} - \mu_{X} \right) / \sigma_{X} \right) \cdot \left(\left(Y_{n} - \mu_{Y} \right) / \sigma_{Y} \right), \tag{1.9}$$

where X represents the vector of measured HRs and Y is the vector of HR values determined from PPG waves, μ and σ denote the mean and the standard deviation of the input vectors X and Y consisting of N elements.

The first stage of comparative measurements was realized in the conditions when the PPG signal from the tested prototype of a PPG sensor was sensed on a little finger, and the oximeter Berry BM1000C [40] used in parallel was worn on an index finger. This type of an OXI device works in a transmittance mode and enables transfer and recording of a PPG signal via BT connection to a control device. There are simultaneously calculated and displayed arterial blood oxygen saturation (SpO₂), perfusion index (PI), and HR values – see an experimental arrangement photo in Fig. 1.15a (the tablet Lenovo M10 was used in these measurements). In the second part of comparative measurements, the automatic blood pressure monitor BP A150-30 AFIB by Microlife AG [41] was applied. To prevent negative influence of an inflated pressure cuff of the BPM on a tested person's blood system, the PPG signal was picked up from an index finger of the opposite hand as documented by the arrangement photo in Fig. 1.15b. The PPG signal recording as well as the measurement by an oximeter always lasted with duration $T_{\text{DUR}} = 80$ sec. The evaluation of the HR precision was performed numerically (by the mean HR_{DIFF} values per a PPG sensor prototype), and also graphically using the correlation scatter plots (see graphs in Fig. 1.16) and Bland-Altman plots (see Fig. 1.17).



Fig. 1.15. Arrangements of comparative measurements: a) Parallel sensing of the PPG signal by the PPG-BLE sensor and via the OXI with BT data transfer to a tablet (both placed on the same hand); b) Parallel HR measurement by the BPM device (pressure cuff on the right arm) and PPG signal sensing by the PPG-PS1 sensor worn on the opposite left hand.

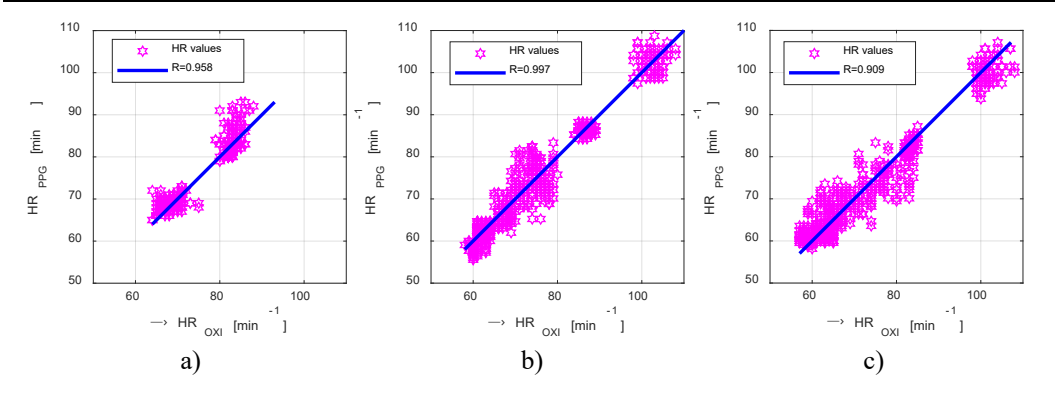


Fig. 1.16. Scatter plots of correlations between the values measured (HR_{OXI}) and determined from PPG signals (HR_{PPG}) together with the calculated R coefficient using: a) PPG-EP; b) PPG-PS1; c) PPG-BLE sensors.

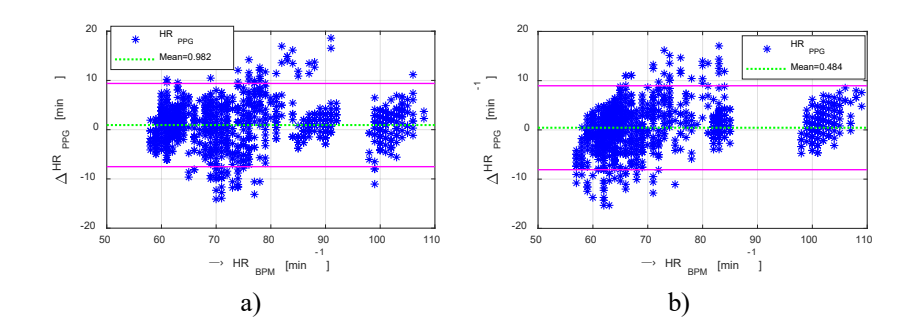


Fig. 1.17. Resulting Bland-Altman plots of the HR determination accuracy from PPG waves with parallel HR measurement by a BPM device for: a) PPG-2Tp; b) PPG-3p sensors.

1.5. Conclusions and Future Work

Wearable PPG sensor prototypes described in this study were developed especially for measurement in the weak magnetic field environment. Before starting this development, we had already tested commercial "fitness bracelets" and smart watches. These types of devices work in the reflectance mode and produce HR parameter values that are not very precise and are not designed for function in the conditions of the running MRI tomograph. In addition, majority of these commercial devices are not able to send the PPG signal samples to an external device (the HR values only). For our purpose we need to evaluate fast and slow changes of the heart rate as well as changes in the width of systolic/diastolic pulses to determine special PPG signal properties (for example the Oliva-roztocil index which has been used as an approach to pain quantification [42]). The heart pulse transmission parameters (PTT and PWV) seem to be sufficient for this task. These parameters are successfully usable for stress detection, evaluation, and classification – for mapping and monitoring of these objective clinical states observed in people who are

exposed to negative factors for a short period of time – such as during scanning inside the MRI device.

From experimental studies and practical measurements follows that the actual state of the skin surface including a color, a temperature, and other factors have influence on the quality and properties of the sensed PPG signals. Thus, PPG sensors are supplemented by a contact thermometer to carry out the measurement of the skin temperature to map its changes during an experiment. In addition, the precision of the determined PPG wave features depends also on the actual position of the optical sensor and the contact pressure exerted in the place of the sensor. To analyze this influence, force-sensitive resistors (FSR) can be successfully used to measure the localized physical pressure.

For this reason, we plan in the near future to develop a new wearable PPG sensor including also an integrated contact thermometer and an FSR element for contact pressure measurement. Next, for different contact forces on a finger/wrist, we will realize a measurement of PPG signals with the aim to collect a database of PPG wave records. Then, we will analyze the determined PPG wave features to make practical recommendation about setting the contact force which is important for long-time measurement experiments inside the MRI device.

The insufficient precision of manual measurement of distances Dx can have negative influence on the inaccuracy of PWV values. It could be improved by a semi-automatic approach which is usually used for determination of distances from images.

Finally, we are fully aware that only a small group of tested subjects (typically up to 15 persons) participated in measurement experiments with our developed PPG sensors, so the obtained results and conclusion from the performed observation cannot be generalized. It was caused by several factors and problems. First of all, the open-air MRI device Esaote Opera [9] directly usable for our experiments with PPG signal(s) recording is devised for standard medical practice, and our institute does not hold a certificate for real patient examination. Therefore, it can be used for non-clinical and non-medical research only. We believe that we will be able to establish close cooperation with the nearest medical centers in our country (in Bratislava), Austria (in Vienna), or Czech Republic (Brno, Prague, etc.) to solve this limitation.

Acknowledgements

This work was funded by the Slovak Scientific Grant Agency project VEGA2/0004/23.

References

- [1]. L. Schickhofer, J. Malinen, M. Mihaescu, Compressible flow simulations of voiced speech using rigid vocal tract geometries acquired by MRI. *Journal of the Acoustical Society of America*, Vol. 145, 2019, pp. 2049-2061.
- [2]. M. Masqsood, F. Nazir, U. Khan, F. Aadil, H. Jamal, I. Mehmood, O. Song, Transfer learning assisted classification and detection of Alzheimer's disease stages using 3D MRI scans, *Sensors*, Vol. 19, 2019, 2645.

- [3]. M. Filippi, P. Preziosa, M. A. Rocca, Brain mapping in multiple sclerosis: Lessons learned about the human brain, *NeuroImage*, Vol. 190, 2019, pp. 32-45.
- [4]. R. A. Leijendekkers, M. A., Marra, M. J. M. Ploegmakers, G. Van Hinte, J. P. Frölke, H. Van De Meent, N. Verdonschot, Magnetic-resonance-imaging-based three-dimensional muscle reconstruction of hip abductor muscle volume in a person with a transfemoral bone-anchored prosthesis: A feasibility study, *Physiotherapy Theory and Practice*, Vol. 35, Issue 5, 2019, pp. 495-504.
- [5]. J. P. Marques, F. J. Simons, A. G. Webb, Low-field MRI: An MR physics perspective, *Journal of Magnetic Resonance Imaging*, Vol. 49, 2019, pp. 1528-1542.
- [6]. D. L. Prince, J. P. De Wilde, A. M. Papadaki, J. S. Curran, R. I. Kitney, Investigation of acoustic noise on 15 MRI scanners from 0.2 T to 3 T, *Journal of Magnetic Resonance Imaging*, Vol. 13, 2001, pp. 288-293.
- [7]. M. A. Bernstein, K. F. King, X. J. Zhou, Handbook of MRI Pulse Sequences, *Elsevier Academic Press*, Burlington, 2004.
- [8]. L. P. Panych, B. Madore, The physics of MRI safety, *Journal of Magnetic Resonance Imaging*, Vol. 47, 2018, pp. 28-43.
- [9]. E-Scan Opera, Image Quality and Sequences Manual, Revision 830023522, *Esaote S.p.A.*, Genoa, Italy, 2008.
- [10]. J. Přibil, A. Přibilová, I. Frollo, Vibration and noise in magnetic resonance imaging of the vocal tract: differences between whole-body and open-air devices, *Sensors*, Vol. 18, Issue 4, 2018. 1112.
- [11]. A. Moelker, P. A. Wielopolski, P. M. T. Pattynama, Relationship between magnetic field strength and magnetic-resonance-related acoustic noise levels, *Magnetic Resonance Materials in Physics, Biology and Medicine*, Vol. 16, 2003, pp. 52-55.
- [12]. J. Přibil, A. Přibilová, I. Frollo, Comparison of mechanical vibration and acoustic noise in the open-air MRI, *Applied Acoustics*, Vol. 105, April 2016, pp. 13-23.
- [13]. J. Přibil, A. Přibilová, I. Frollo, Comparison of three prototypes of PPG sensors for continual real-time measurement in weak magnetic field, *Sensors*, Vol. 22, Issue 10, 2022, 3769.
- [14]. M. C. Steckner, A review of MRI acoustic noise and its potential impact on patient and worker health, *eMagRes*, Vol. 9, 2020, pp. 21-38.
- [15]. P. Celka, P. H. Charlton, B. Farukh, P. Chowienczyk, J. Alastruey, Influence of mental stress on the pulse wave features of photoplethysmograms, *Healthcare Technology Letters*, Vol. 7, 2020, pp. 7-12.
- [16]. V. Randazzo, J. Ferretti, E. Pasero, A wearable smart device to monitor multiple vital parameters VITAL ECG, *Electronics*, Vol. 9, 2020, 300.
- [17]. A. G. Bonomi, F. Schipper, L. M. Eerikäinen, J. Margarito, R. Van Dinther, G. Muesch, H. M. De Morree, R. M. Aarts, S. Babaeizadeh, D. D. McManus, Atrial fibrillation detection using a novel cardiac ambulatory monitor based on photoplethysmography at the wrist, *Journal of the American Heart Association*, Vol. 7, 2018, e009351.
- [18]. J. Sancho, A. Alesanco, J. García. Biometric authentication using the PPG: a long-term feasibility study, *Sensors*, Vol. 18, 2018, 1525.
- [19]. B. C. Casadei, A. Gumiero, G. Tantillo, L. Della Torre, G. Olmo, Systolic blood pressure estimation from PPG signal using ANN, *Electronics*, Vol. 11, 2022, 2909.
- [20]. Y. J. Wang, C. H. Chen, C. Y. Sue, W. H. Lu, Y. H. Chiou, Estimation of blood pressure in the radial artery using strain-based pulse wave and photoplethysmography sensors, *Micromachines*, Vol. 9, 2018, 556.
- [21]. M. Johnson, R. Jegan, X. Mary, Performance measures on blood pressure and heart rate measurement from PPG signal for biomedical applications, in *Proceedings of the IEEE International Conference on Innovations in Electrical, Electronics, Instrumentation and Media Technology (ICEEIMT'17)*, Coimbatore, India, 3-4 February 2017, pp. 311-315.

- [22]. Y. Xu, W. Zhang, D. Wang, P. Ping, A calibration method for cuffless continue blood pressure measurement using Gaussian normalized pulse transit time, in *Proceedings of the IEEE International Instrumentation and Measurement Technology Conference (I2MTC'18*), Houston, TX, USA, 14-17 May 2018, pp. 1-5.
- [23]. H. Gesche, D. Grosskurth, G. Küchler, A. Patzak, Continuous blood pressure measurement by using the pulse transit time: Comparison to a cuff-based method, *European Journal of Applied Physiology*, Vol. 112, 2012, pp. 309-315.
- [24]. B. Mishra, N. Thakkar, Cuffless blood pressure monitoring using PTT and PWV methods, in *Proceedings of the International Conference on Recent Innovations in Signal Processing and Embedded Systems (RISE'17)*, Bhopal, India, 27-29 October 2017; pp. 395-401.
- [25]. P. H. Charlton, V. Marozas, Wearable photoplethysmography devices, in Photoplethysmography: Technology, Signal Analysis, and Applications (P. A. Kyriacou, J. Allen, Eds.), *Elsevier*, London, UK, 2022, pp. 401-438.
- [26]. M. Nitzan, Z. Ovadia-Blechman, Physical and physiological interpretations of the PPG signal, in Photoplethysmography: Technology, Signal Analysis, and Applications (P. A. Kyriacou, J. Allen, Eds.), *Elsevier*, London, UK, 2022, pp. 319-339.
- [27]. E. Mejía-Mejía, J. Allen, K. Budidha, C. El-Hajj, P. A. Kyriacou, P. H. Charlton, Photoplethysmography signal processing and synthesis, in Photoplethysmography: Technology, Signal Analysis, and Applications (P. A. Kyriacou, J. Allen, Eds.), *Elsevier*, London, UK, 2022, pp. 69-145.
- [28]. A. G. Smith, Introduction to Arduino: A Piece of Cake, *CreateSpace Independent Publishing Platform*, 2011.
- [29]. Arduino UNO R3, https://docs.arduino.cc/hardware/uno-rev3
- [30]. Arduino Nano Official Store, http://arduino.cc/en/Main/ArduinoBoardNano
- [31]. Using the Arduino Pro Mini 3.3V, https://learn.sparkfun.com/tutorials/using-the-arduino-pro-mini-33v
- [32]. Adafruit Metro Mini 328 V2, https://www.adafruit.com/product/2590
- [33]. Arduino and Bluetooth Module HC-06, https://www.aranacorp.com/en/arduino-and-bluetooth-module-hc-06/
- [34]. MLT-BT05 4.1 Bluetooth Serial Communication Module, https://www.techonicsltd.com/product/mlt-bt05-ble4-0/
- [35]. Pulse Sensor Amped Product (Adafruit 1093), World Famous Electronics LLC, Ecommerce Getting Starter Guide, https://pulsesensor.com/pages/code-and-guide
- [36]. Crowtail Pulse Sensor (ER-CT010712P) measure the heart rate of the human, https://rlx.sk/sk/biometric-medical-e-health-sensor-eeg-ekg/5431-crowtail-pulse-sensor-erct010712p
- [37]. Gravity: PPG Heart Rate Monitor Sensor for Arduino (Analog/Digital). https://www.dfrobot.com/product-1540.html
- [38]. Easy Pulse Sensor (Version 1.1), Overview Embedded Lab, http://embedded-lab.com/blog/easy-pulse-version-1-1-sensor-overview
- [39]. Easy Pulse Mikro A Mikrobus Compatible Pulse Sensor Embedded Lab, https://www.embedded-lab.com/blog/easy-pulse-mikro/#more-11519
- [40]. China Berry Hospital Oxycare Pulse Oximeter for Kids, https://berrymedical.en.made-in-china.com/product/zsuQEvPLsqcJ/Ch
- [41]. Microlife BP A150 AFIB, https://www.microlife.cz/produkty/krevni-tlak/automaticke-tlakomery/bp-a150-afib
- [42]. J. Pitha, P. Pithova, K. Roztocil, K. Urbaniec, Oliva-roztocil index, specific parameter of vascular damage in women suffering from diabetes mellitus, *Atherosclerosis*, Vol. 263, 2017, e275.